Journal of Inflammation Research

Dovepress
Taylor & Francis Group

Open Access Full Text Article

ORIGINAL RESEARCH

Hyperoside Attenuates Lupus Nephritis-Associated Mesangial Cell Apoptosis via the P53/XAF1 Pathway: Integrative Bioinformatics and In Vitro Validation

Lili Cheng[1,*], Zhongfu Tang[1,*], Ming Li[1], Junjie Chen[2], Chuanbing Huang[1]

[1]Department of Rheumatology and Immunology, The First Affiliated Hospital of Anhui University of Chinese Medicine, Hefei, Anhui, 230012, People's Republic of China; [2]College of Traditional Chinese Medicine, Anhui University of Chinese Medicine, Hefei, Anhui, 230012, People's Republic of China

*These authors contributed equally to this work

Correspondence: Chuanbing Huang, Department of Rheumatology and Immunology, First Affiliated Hospital of Anhui University of Traditional Chinese Medicine, Hefei, Anhui Province, 230038, People's Republic of China, Tel +86-15156986428, Email Chuanbinh@163.com

Objective: This study aimed to explore potential molecular targets and pathways of Hyp in LN using integrative bioinformatics and network pharmacology, and to provide in vitro validation of key mechanistic hypotheses in an IFN-α–induced mesangial-cell injury model.

Methods: Differential expression analysis was performed on multiple datasets to identify LN-related target genes. Integrative approaches including machine learning algorithms, network pharmacology, and molecular docking were employed to explore the binding interactions between Hyp and target proteins. In vitro experiments were conducted to validate the mechanism by which Hyp intervenes in glomerular mesangial cell apoptosis.

Results: A total of 18 genes were identified as potential targets involved in Hyp-induced modulation of LN progression. Machine learning SHAP analysis identified 5 core genes (STAT1, RSAD2, OAS3, GBP1, XAF1) as key regulators. Molecular docking simulations revealed specific binding between Hyp and each target protein, with particularly strong binding affinity between Hyp and XAF1. Cellular experimental results demonstrated that Hyp could inhibit the P53/XAF1 signaling pathway, downregulate the expression of apoptosis-related proteins, and thereby alleviate glomerular mesangial cell apoptosis.

Conclusion: Hyp attenuated IFN-α–induced glomerular mesangial cell apoptosis by suppressing the P53/XAF1 signaling pathway, suggesting a potential therapeutic mechanism in LN. These integrative bioinformatics and in vitro findings provide a rationale for future in vivo validation and clinical translation.

Keywords: hyperoside, lupus nephritis, apoptosis, P53/XAF1, glomerular mesangial cells

Introduction

Systemic lupus erythematosus (SLE) is an autoimmune disease characterized by multi-organ damage. Approximately 30–60% of adult SLE patients and up to 70% of pediatric SLE patients develop lupus nephritis (LN), which severely threatens patients' health.[1] LN is one of the most severe and common complications of SLE,[2] and a major risk factor for morbidity and mortality, with the incidence of progression to end-stage renal disease (ESRD) ranging from 4.3% to 10.1%.[3] The pathogenesis of LN involves complex immune dysregulation, with key pathways including type I interferon signaling, calcineurin activation, and dysfunction of B and T cells.[4] Currently, clinical treatment for LN mainly relies on high-dose corticosteroids and immunosuppressive drugs such as cyclophosphamide and mycophenolate mofetil.[5] However, while these traditional therapies exert therapeutic effects, they also bring numerous side effects, including increased risk of infection, osteoporosis, abnormalities in blood glucose and lipid metabolism, and gonadal function

https://doi.org/10.2147/JIR.S586751
Received: 5 December 2025
Accepted: 3 March 2026
Published: 12 March 2026

damage, which seriously affect patients' quality of life and long-term prognosis. Thus, the development of safer and more effective therapeutic strategies has become a critical issue urgently needing resolution in the medical field.

Abnormal cell apoptosis is one of the core pathological links in renal injury of LN, involving various cell types such as immune cells and intrinsic renal cells, and is closely related to signaling pathways regulated by multiple factors including immune complexes, cytokines, and non-coding RNAs. Mesangial cells (MCs) account for 30–40% of the total glomerular cells. In addition to forming the filtration membrane, MCs can secrete cytokines, growth factors, and extracellular matrix, and phagocytose macromolecules and apoptotic cells to restore glomerular stability.[6] As an important form of programmed cell death, glomerular mesangial cell apoptosis plays a crucial role in the occurrence and development of LN. In LN patients, glomerular mesangial cells are attacked by various inflammatory mediators, cytokines, and autoantibodies, leading to the activation of a series of apoptosis-related signaling pathways and induction of apoptotic imbalance. Excessive mesangial cell apoptosis disrupts the normal structure of the glomerulus, induces mesangial matrix proliferation, thereby impairing the filtration function of the glomerulus and triggering typical clinical symptoms of LN such as proteinuria and hematuria.[7] Therefore, in-depth study of the mechanism underlying glomerular mesangial cell apoptosis in LN is of great significance for revealing the pathogenic essence of LN and identifying effective therapeutic targets.

Hyperoside, a natural flavonoid compound, is widely present in the traditional Chinese medicine Cuscutae Semen. With its multiple pharmacological activities including anti-inflammatory, immunomodulatory, anti-apoptotic, and anti-oxidative stress effects, it has shown significant potential therapeutic value in autoimmune diseases.[8,9] Studies have found that hyperoside improves diabetic nephropathy by promoting the polarization of macrophages from M1 to M2 phenotype and the differentiation of CD4+ T cells into Th2 and Treg populations;[10] it protects HL-1 cardiomyocytes and alleviates apoptosis by inhibiting the ASK1/p38 signaling pathway.[11] However, whether hyperoside can protect against glomerular mesangial cell apoptosis in LN and its underlying mechanism have not been fully elucidated. Based on the protective effect of hyperoside on glomerular mesangial cells and its anti-apoptotic pharmacological activity, we hypothesize that hyperoside may exert a potential therapeutic effect on LN by regulating glomerular mesangial cell apoptosis. This hypothesis opens up a new direction for LN treatment research and provides an important theoretical basis for the application of hyperoside in the treatment of renal diseases.

In this study, we systematically integrated multiple cutting-edge technologies and experimental methods including network pharmacology, machine learning, SHAP analysis, molecular docking, and cellular experiments to comprehensively and in-depth explore and clarify the potential molecular mechanism of hyperoside in the treatment of LN, aiming to fully reveal its potential value as a candidate drug for LN therapy.

Materials and Methods

Acquisition of Disease-Related Targets

Four transcriptomic datasets of SLE and LN (GSE10325, GSE46907, GSE50772, and GSE99967) were collated from the NCBI GEO database.[12] GSE10325 and GSE46907 served as the discovery cohort, while the remaining two datasets (GSE50772, GSE99967) constituted the validation cohort. To mitigate batch effects, a multi-stage normalization pipeline was implemented: Surrogate Variable Analysis (SVA): The SVA package was used to model and adjust for potential confounding factors in the discovery cohort. ComBat harmonization: Residual batch variations were further corrected through a parametric empirical Bayes framework. Principal Component Analysis (PCA) after correction showed improved clustering of samples across batches in the reduced-dimensional space, confirming the success of data harmonization. All included GEO cohorts were derived from adult patients and were not designed as paediatric/childhood-onset lupus nephritis cohorts; therefore, age-stratified comparisons (paediatric vs adult) could not be performed based on the available public metadata.[13]

Acquisition of Chemical Composition and Targets of Hyperoside (Hyp)

The chemical composition and targets of Hyp were obtained through multi-database integration. The SMILES string of Hyp (C1=CC(=C(C=C1C2=C(C(=O)C3=C(C=C(C=C3O2)O)O)O[C@H]4C@@HO)O)O) was retrieved from the

PubChem database[14] (https://pubchem.ncbi.nlm.nih.gov/). Target prediction was combined with three databases: ChEMBL database[15] (https://www.ebi.ac.uk/chembl/), SwissTargetPrediction[16] (http://www.swisstargetprediction.ch), and SEA database[17] (https://sea.bkslab.org/). All predicted targets were restricted to the Homo sapiens proteome. Conversion between proteins was performed using the UniProt database (https://www.uniprot.org/).

Differential Gene Expression Analysis

Transcriptomic data were analyzed using the limma package.[18] Differential Expression Genes (DEGs) were identified with thresholds of $P < 0.05$ and $|\log2FC| > 0.585$ (1.5-fold change). Results were visualized using the ggplot2 and pheatmap packages.

Weighted Gene Co-Expression Network Analysis

A scale-free co-expression network was constructed using WGCNA (v1.72). Genes with a standard deviation < 0.5 were excluded; samples and genes with more than 5% missing values were removed using the "goodSamplesGenes" function. Samples were hierarchically clustered based on Euclidean distance, with an edge height of 20,000 to remove outlier samples (minClusterSize = 10). A power scan from 1 to 20 was performed, and the minimum power value with a scale-free topology fitting index $R^2 > 0.85$ and a stable average connectivity was selected as the soft threshold. Gene connectivity was measured using the Topological Overlap Matrix (TOM), and initial modules were obtained by dynamic cutting (deepSplit = 2, minModuleSize = 60); Module Eigengenes (ME) were clustered, and similar modules with a height < 0.25 were merged to obtain the final merged functional modules. Pearson correlation and corresponding P values between MEs and binary traits (Control/Treat) were calculated, and modules with $|r| > 0.5$ and $P < 0.05$ were considered significantly associated modules. Within the significantly associated modules, hub genes were screened with thresholds of Module Membership (MM) > 0.8 and Gene Significance (GS) > 0.2. Expression normalization was performed using limma; all graphs (sample clustering, soft threshold evaluation, module clustering, module-trait heatmap, MM-GS scatter plot) were output using built-in WGCNA functions.[19]

Identification of Hyp-LN Targets and Functional Enrichment Analysis

Core Hyp-LN targets were identified by intersecting DEGs/WGCNA hub genes with Hyp-predicted targets, and visualized using a Venn diagram. GO (biological process, cellular component, molecular function) and KEGG pathway analyses were performed using the clusterProfiler package[20] ($P < 0.05$) to clarify the potential role of Hyp in the pathogenesis of LN.

Screening of Core Genes Based on Machine Learning

To systematically identify LN diagnostic biomarkers related to Hyp, we established a comprehensive machine learning prediction framework integrating multiple algorithms. Based on the expression matrices of the training set and independent test set, 9 integrated/single algorithms (RF, XGBoost, GBM, mboost, plsRglm, BART, SVM, randomForestSRC, glmnet) were used to construct binary classification models. The workflow was as follows: Common genes in the training and test sets were selected, and Z-score standardization was performed by cohort for data quality control; within each single algorithm, genes were ranked by "variable importance", and ≥ 5 genes were retained; Model training: 10-fold cross-validation was repeated with seed=123, and the optimal model was selected based on the highest AUC; AUC was calculated in the training and test sets respectively, and a cohort-algorithm heatmap was drawn; the model with the highest average AUC and its characteristic gene list were retained for subsequent functional annotation and validation.[21]

SHAP Analysis

Given that traditional machine learning models are often regarded as "black boxes" with poor interpretability, we introduced the SHapley Additive exPlanations (SHAP) algorithm in this study. The core function of this algorithm is to quantify the contribution of each feature gene to the model's prediction results. Specifically, it assigns a specific SHAP

value to each feature, which allows us to conduct an interpretable assessment of how each gene impacts the model's prediction outcomes, thereby overcoming the limitation of the model's opacity.

Molecular Docking

To verify the potential binding interactions between Hyp and the screened core genes (STAT1, RSAD2, OAS3, GBP1, XAF1), we carried out a full-scale molecular docking analysis. The ligand structures in SDF format and the 3D protein models of the core targets were obtained from the PubChem and UniProt databases, respectively. Prior to docking, we preprocessed the protein structures by removing water molecules and adding hydrogen atoms. The docking grid was centered on the predicted active site of the protein, and its size was adjusted based on the ligand's size and the predicted binding mode. All docking operations were completed using AutoDock Vina and PyMOL.

Drugs and Reagents

Hyperoside (B20631) was purchased from Shanghai Yuanye Biotechnology Co., Ltd. (Shanghai, China). IFN-α (HY-P70241) was purchased from MedchemExpress (USA).

Cell Culture and Transient Transfection

Human glomerular mesangial cells (HMCs; catalog no. HUM-iCell-u002) were purchased from Cyagen Biosciences (Shanghai, China) and cultured according to the supplier's instructions. Cells were cultured in DMEM medium (SH30022.01, cytiva, USA) containing 1% penicillin-streptomycin (C0222, Beyotime, China) and 10% FBS (SH30256.01, cytiva, USA) at 37°C with 5% CO2. Transfection of siRNA or overexpression plasmids was performed according to the manual of Lipofectamine 2000 (2307486, Invitrogen, USA). siRNA and overexpression plasmids were purchased from General Biosystems (Anhui, China). Sequence information is provided in Supplementary Table 1.

CCK-8 Assay

Cell viability was detected using the CCK-8 assay kit (BS350B, Biosharp). Logarithmic phase cells were digested with trypsin (C0201, Beyotime, China), terminated, centrifuged to collect, and made into cell suspension. Cell concentration was adjusted to 4×104/mL by cell counting. After preparing the cell suspension, it was gently mixed, 8000 cells were added to each well, and the edge wells were filled with sterile PBS (SH30256.01, cytiva, USA). The inoculated cell culture plate was placed in an incubator overnight and observed under an inverted microscope (CKX31, OLYMPUS, Japan). Drugs were added at different concentrations, and after culturing for different times, 10 μL of CCK-8 was added to each well and incubation continued for 1–4 hours. The absorbance value of each well was measured at 450 nm using a microplate reader, and the cell viability of each group was calculated. The calculation formula for cell viability in each group was as follows: Cell viability $=[(\text{Experimental well} - \text{Blank well})/(\text{Control well} - \text{Blank well})]$.

Flow Cytometry

Cells were collected by centrifugation at 800–1000×g for 5 minutes at 4°C, washed twice with cold PBS, and counted. $1–10\times10^5$ cells were resuspended in 500 μL of freshly prepared 1×Binding Buffer, 5 μL of Annexin V-FITC and 10 μL of PI were added, gently mixed, and incubated at room temperature in the dark for 5 minutes. Detection was performed using a calibrated flow cytometer (CytoFLEX, Beckman) within 30 minutes, and 10,000–20,000 cell events were collected. Signals were calibrated using negative controls and single-stain controls. The total apoptosis rate was the sum of the proportions of early apoptotic (Annexin V-FITC+/PI^-) and late apoptotic/necrotic (Annexin V-FITC+/PI^+) cells. The entire experiment was performed at low temperature in the dark to avoid cell damage and fluorescence quenching.

TUNEL (Fluorescence) Staining

The primary TUNEL apoptosis detection kit (E-CK-A320, Elabscience) was used to evaluate the apoptosis of HMC cells according to the manufacturer's protocol. Cells were gently washed 3 times with PBS-T; then fixed with 4% paraformaldehyde for 20 minutes, gently washed 3 times with PBS-T again, followed by 3 washes with PBS; TUNEL detection

solution was prepared at a ratio of TdT enzyme to fluorescence labeling solution of 1:9, added to the cell samples, and incubated in a 37°C incubator for 30–60 minutes; after incubation, washed 3 times with PBS, and finally mounted with anti-fluorescence quenching mounting medium containing DAPI (P0131, Beyotime). After mounting, fluorescence sections were scanned using a digital slide scanner (Pannoramic MIDI, 3DHISTECH, Hungary). Fluorescence intensity was further analyzed using ImageJ software. The ratio of TUNEL-positive nuclei to total DAPI-stained nuclei was calculated to evaluate the apoptosis rate.

Quantitative Reverse Transcription Polymerase Chain Reaction (qRT-PCR)

Total cellular RNA was extracted according to the manual of TRIzol reagent (15596018CN, Life Technologies, USA). For RT-PCR analysis, cDNA was generated using the PrimeScript™ RT reagent Kit with gDNA Eraser (RR047A, TaKaRa, Japan). cDNA, fluorescent dye (Novostart SYBR qPCR SuperMix Plus, Novoprotein, E096-01B, Novoprotein, Suzhou, China), primers, and PCR reagents were mixed and added to the reaction plate, and analyzed using a real-time fluorescent quantitative PCR instrument (Thermo Scientific, PIKOREAL 96, Finland). The Relative Quantification Study method was selected, and the calculation method was 2-ΔΔCt to obtain the relative mRNA level. PCR primers were purchased from Shanghai Sangon Biotech Co., Ltd. (Shanghai, China). Primer information for each target is shown in Table 1.

Western Blot Analysis

Cell samples (approximately 1×10^5 cells) were collected, and 600 μL of RIPA cell lysis buffer (P0013B, Beyotime, China) containing 0.6 mM PMSF was added for lysis. Centrifuged at 12,000 ×g for 15 min. The supernatant was collected, which contained total cellular protein. Protein samples were separated by SDS-PAGE electrophoresis according to molecular weight, and then transferred from the gel to PVDF membranes (IPVH00010, Millipore, USA) by electrotransfer. Subsequently, blocking was performed with BSA or non-fat milk to prevent non-specific binding of antibodies. The membrane was first incubated with specific primary antibodies, then with enzyme-labeled secondary antibodies. Finally, proteins were detected using an ECL luminescence kit (BL520A, Biosharp, China) with reference to the relevant instructions. Information on related antibodies is provided in Supplementary Table 2.

Statistical Analysis

SPSS 26.0 software was used for statistical analysis of experimental data, and ImageJ software was used for analysis of microscope imaging results. GraphPad Prism 8 software was used for graphing. For measured data conforming to normal distribution and homogeneity of variance, independent samples *t*-test was used for comparison between two groups, and one-way analysis of variance was used for comparison among multiple groups. Statistical significance was defined as $^{**}P < 0.01$, $^{*}P < 0.05$.

Results

Identification of LN-Related Target Genes

To minimize batch effects that might interfere with the accuracy of subsequent analyses, we integrated the GSE10325 and GSE46907 datasets and implemented a comprehensive normalization process for the gene expression matrix. The cluster box plots and Principal Component Analysis (PCA) results demonstrated that the data distribution was notably

Table 1 Primers for Each Target

Gene	Amplicon Size (bp)	Forward Primer (5'→3')	Reverse Primer (5'→3')
β-actin	96	CCCTGGAGAAGAGCTACGAG	GGAAGGAAGGCTGGAAGAGT
p53	152	GTCTACCTCCCGCCATAA	GCAAGCAAGGGTTCAAAG
XAF1	175	AAACTCCGTCTCCGCTAA	GCAGAGTCTCGCTTGGTT

https://doi.org/10.2147/JIR.S586751

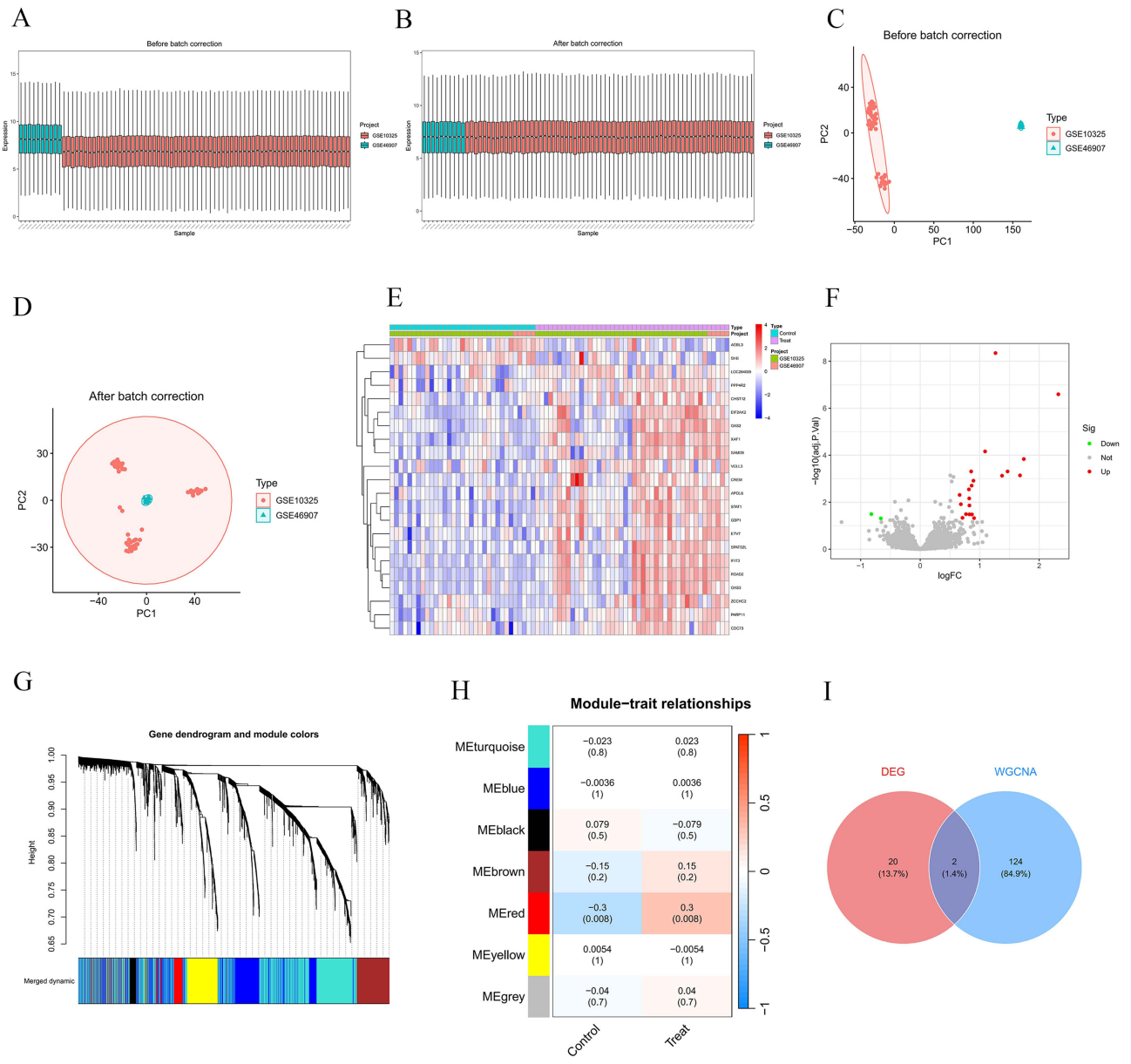

Figure 1 Identification of LN-related target genes. (**A**) Sample cluster box plot before batch correction; (**B**) Sample cluster box plot after batch correction; (**C**) Principal Component Analysis (PCA) plot before batch correction; (**D**) Principal Component Analysis (PCA) plot after batch correction; (**E**) Heatmap of differentially expressed genes; (**F**) Volcano plot of differentially expressed genes; (**G**) Gene clustering tree and module colors of WGCNA; (**H**) Correlation heatmap between WGCNA modules and phenotypes; (**I**) Venn diagram of Differentially Expressed Genes (DEGs) and WGCNA module genes.

improved after normalization, and the normalized dataset exhibited a more distinct sample clustering pattern (Figure 1A–D).

Through differential expression analysis, we screened out 22 genes that showed significant expression alterations in LN. We visualized these expression variations using a heatmap and a volcano plot (Figure 1E and F). For Weighted Gene Co-Expression Network Analysis (WGCNA), we constructed a Topological Overlap Matrix (TOM) and conducted hierarchical clustering to define co-expression modules. This analysis yielded seven distinct gene modules, each marked with a unique color for intuitive visualization (Figure 1G).

Subsequently, we performed module-trait relationship analysis and found that the red module had a significant association with LN ($P < 0.05$) (Figure 1H). By combining the differentially expressed genes from conventional

differential analysis with the module genes obtained from WGCNA (after removing duplicate genes), we finally identified a set of 146 LN-related genes (Figure 1I).

Potential Targets of Hyp and LN

Potential biological targets of Hyp were predicted from three databases (ChEMBL, SEA, and SwissTargetPrediction), and after data fusion and deduplication, a total of 165 unique potential targets were identified (Figure 2A). Intersection analysis between Hyp target proteins and LN-related genes identified 18 potential key targets involved in Hyp-inhibited LN progression (Figure 2B), and the intersecting genes are shown in Figure 2C. GO and KEGG enrichment analyses of the intersecting targets revealed comprehensive molecular insights. GO analysis showed significant enrichment in biological processes (such as viral defense response, regulation of viral life cycle), cellular components (such as cyclin complex), and molecular functions (such as histone kinase activity) (Figure 2D), but "biological process" was the main enrichment direction of differentially expressed genes (Figure 2E). KEGG pathway analysis emphasized that differentially expressed genes are mainly involved in viral infection response, immune signal transduction (NOD-like signaling pathway), as well as basic biological processes such as cell proliferation, apoptosis, and senescence (P53 signaling pathway) (Figure 2F).

Identification of Core Genes in Hyp-Treated LN

Through comprehensive machine learning analysis, we constructed multiple sets of prediction models to identify core genes of LN. Integrated models such as Stepglm showed excellent performance in both training and validation phases, among which the Stepglm algorithm exhibited the optimal performance (Figure 3A). SHAP interpretability analysis further revealed the functional contributions of genes, among which Signal Transducer and Activator of Transcription 1 (STAT1) (SHAP value=0.386), Radical S-Adenosylmethionine Domain Containing 2(RSAD2)(SHAP value=0.227), 2',5'-Oligoadenylate Synthetase 3(OAS3) (SHAP value=0.193), Guanylate Binding Protein 1(GBP1) (SHAP value=0.158), X-linked Inhibitor of Apoptosis Protein-Associated Factor 1(XAF1)(SHAP value=0.086), etc, showed

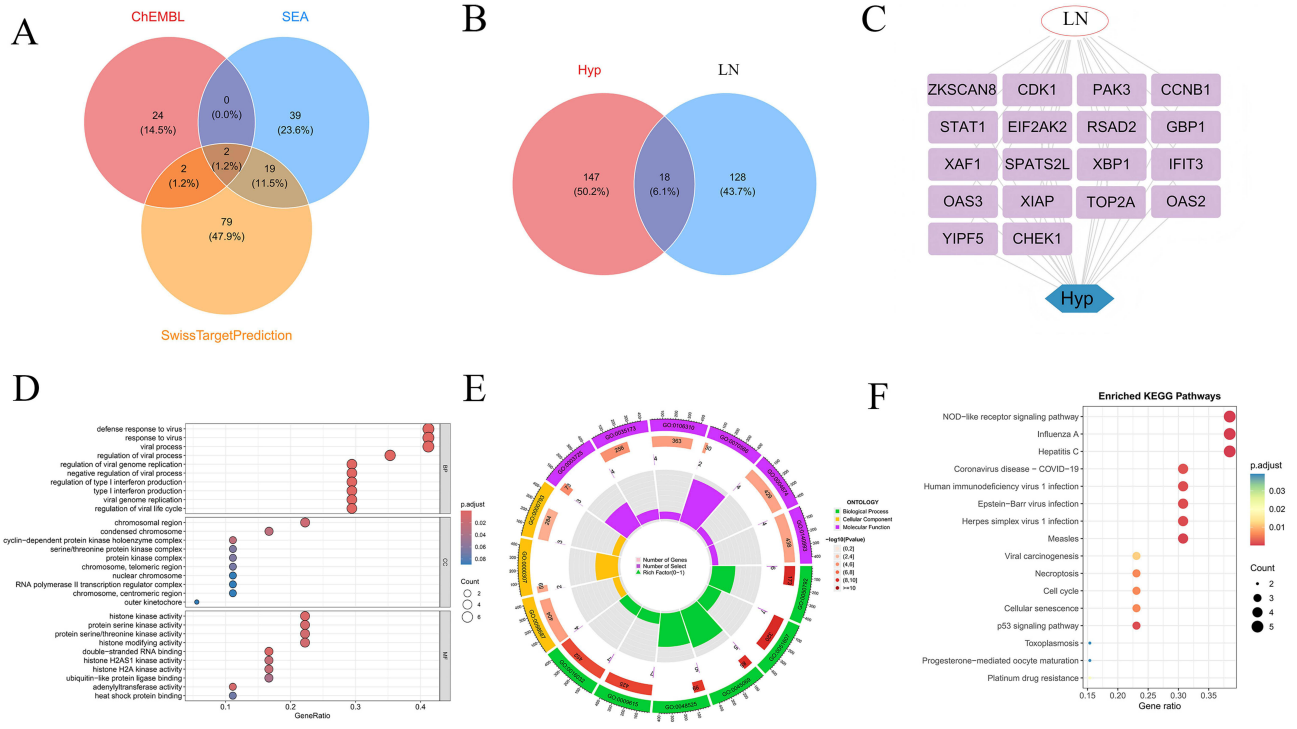

Figure 2 Potential targets of Hyp and LN. (**A**) Venn diagram of target intersections from 3 databases; (**B**) Venn diagram of intersections between LN-related genes and Hyp-related genes; (**C**) Co-gene association network of LN and Hyp; (**D**) Bubble plot of GO enrichment analysis; (**E**) Chord diagram of GO enrichment; (**F**) Dot plot of KEGG pathway enrichment analysis.

https://doi.org/10.2147/JIR.S586751

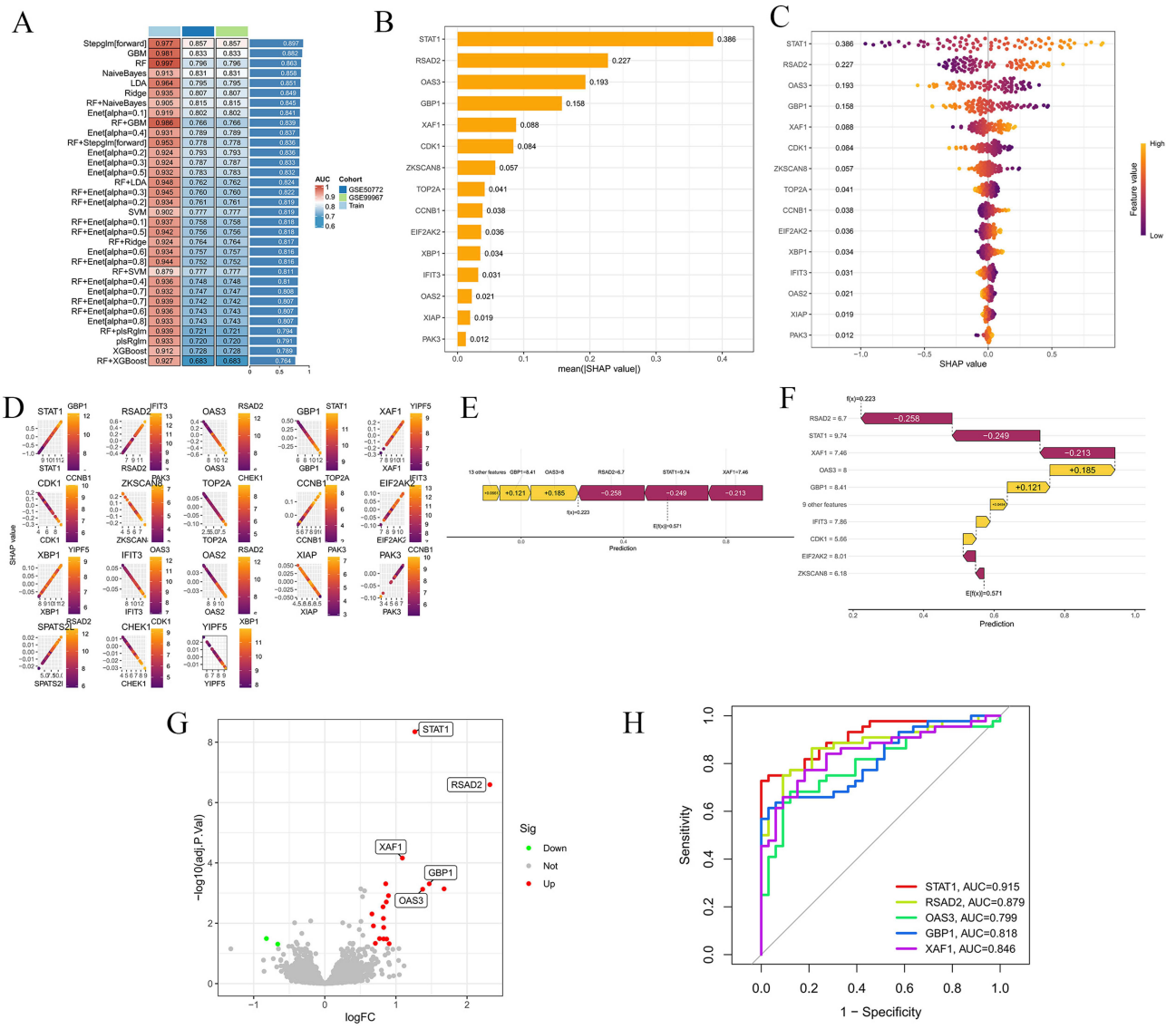

Figure 3 Identification of core genes in Hyp-treated LN. (**A**) Performance comparison heatmap of different models; (**B**) Ranking of average SHAP values of core genes; (**C**) SHAP feature importance scatter plot; (**D**) SHAP dependence plot of individual genes; (**E** and **F**) SHAP decision plots; (**G**) Volcano plot of differentially expressed genes; (**H**) ROC curve analysis of genes.

core contribution capabilities (Figure 3B). High expression of core genes such as STAT1 is key to enhancing model prediction contribution, and it also reveals the correlation between gene expression levels and predictive regulation directions (Figure 3C). Different screened genes showed differential regulatory effects on prediction results at different expression levels (Figure 3D). RSAD2 (−0.258), STAT1 (−0.249), XAF1 (−0.213) are the main negative regulators of SHAP predicted values, while genes such as OAS3 (+0.185) and GBP1 (+0.121) play positive regulatory roles (Figure 3E and F). Volcano plots of differential expression of genes such as STAT1, RSAD2, GBP1, and XAF1 are intuitively presented in Figure 3G. ROC curve analysis (Figure 3H) showed that the AUC values of STAT1, RSAD2, GBP1, and XAF1 are all higher than 0.8, verifying their good diagnostic potential. These results collectively confirm the key role of core genes in disease prediction and molecular mechanisms.

Molecular Docking Verification of Hyp-Core Gene Interactions

To verify the potential binding interactions between Hyp and the identified core genes (STAT1, RSAD2, OAS3, GBP1, XAF1), we performed comprehensive molecular docking analysis. The results indicated that Hyp had strong binding

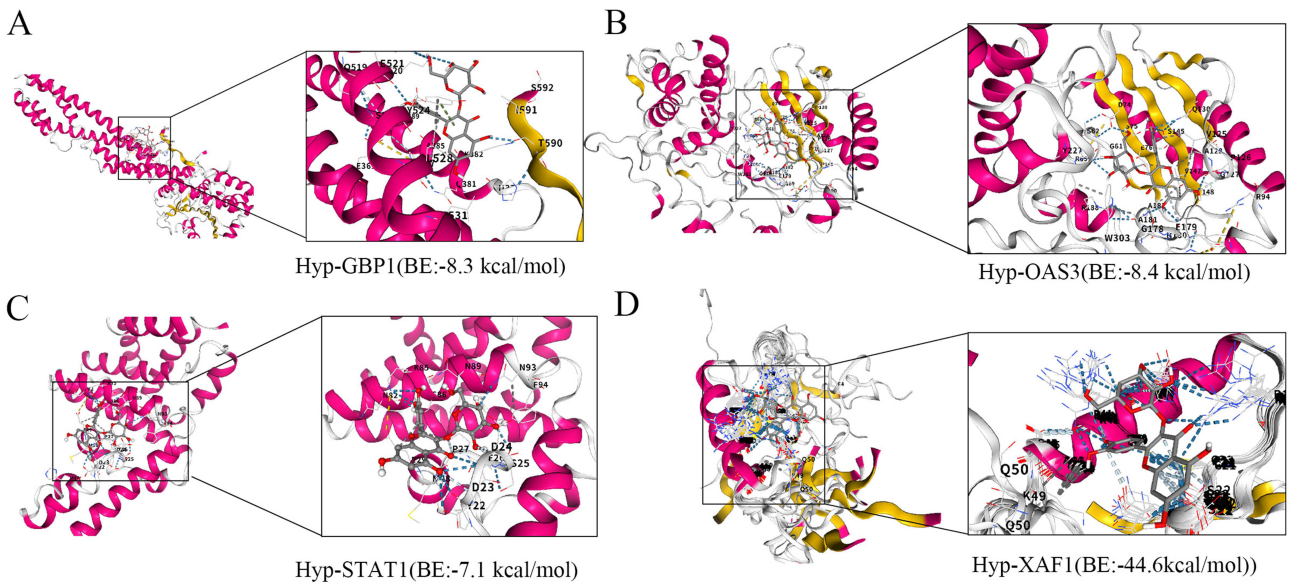

Figure 4 Molecular docking verification of Hyp-core gene interactions. (**A**) Hyp-GBP1; (**B**) Hyp-OAS3; (**C**) Hyp-STAT1; (**D**) Hyp-XAF1.

affinity with four of the five target proteins (excluding RSAD2), and the binding energy of these interactions was consistently below −5 kcal/mol, which implies that the molecular binding between Hyp and these target proteins is stable and can occur spontaneously. Among these targets, Hyp exhibited an extremely strong binding force with XAF1 (Figure 4). These findings provide structural evidence to support the direct molecular interactions between Hyp and the core LN targets identified by our machine learning approach. Based on the above analysis, we speculate that XAF1 may be the core target of Hyp in intervening LN. Combined with literature and KEGG enrichment results, the P53 signaling pathway may be the key signaling pathway.

Hyp Effectively Inhibits HMC Apoptosis and XAF1 Expression

We used HMC cells for in vitro experimental verification. First, the optimal concentration and time of IFN-α were determined using cell viability. CCK-8 results showed that with the increase of IFN-α concentration, the viability of HMC cells continued to decrease (Figure 5A), and the apoptosis rate of HMC cells gradually increased (Figure 5B). Therefore, according to the IC50 value, 500 U/mL IFN-α intervention for 48h was selected as the model for subsequent experiments. To explore the renal protection mechanism related to Hyp, we intervened with low, medium, and high doses of Hyp (25 μg/mL, 50 μg/mL, 100 μg/mL) respectively. CCK-8 results showed that Hyp significantly increased cell viability in a dose-dependent manner (Figure 5C). Flow cytometry results showed that Hyp intervention significantly reduced the apoptosis rate (Figure 5D and E). TUNEL staining results also showed this characteristic (Figure 5F). WB results showed that the expression levels of Cleaved Caspase-3 and Cleaved PARP proteins were significantly down-regulated in the Hyp intervention group compared with the model group (Figure 5G–I). The above results indicate that Hyp can effectively inhibit HMC cell apoptosis. At the same time, PCR and WB results showed that the relative mRNA expression level of XAF1 in the model group was significantly higher than that in the control group, while Hyp intervention significantly reduced the expression of XAF1 in a dose-dependent manner (Figure 5J and K).

P53/XAF1 Mediates HMC Apoptosis

Previous GO and KEGG enrichment analyses found that the P53 signaling pathway was mainly enriched. Subsequently, we reduced the expression of P53 in HMC cells by transfecting P53-specific siRNA to explore its role in regulating XAF1 expression. Based on the transfection efficiency of si-P53, we selected si-P53 2# for subsequent experiments (Supplementary Figure 1A). Previous studies have shown that p53, as a transcription factor, can specifically bind to the p53 response element in the promoter region of the XAF1 gene, directly driving the transcription of the XAF1 gene and

https://doi.org/10.2147/JIR.S586751

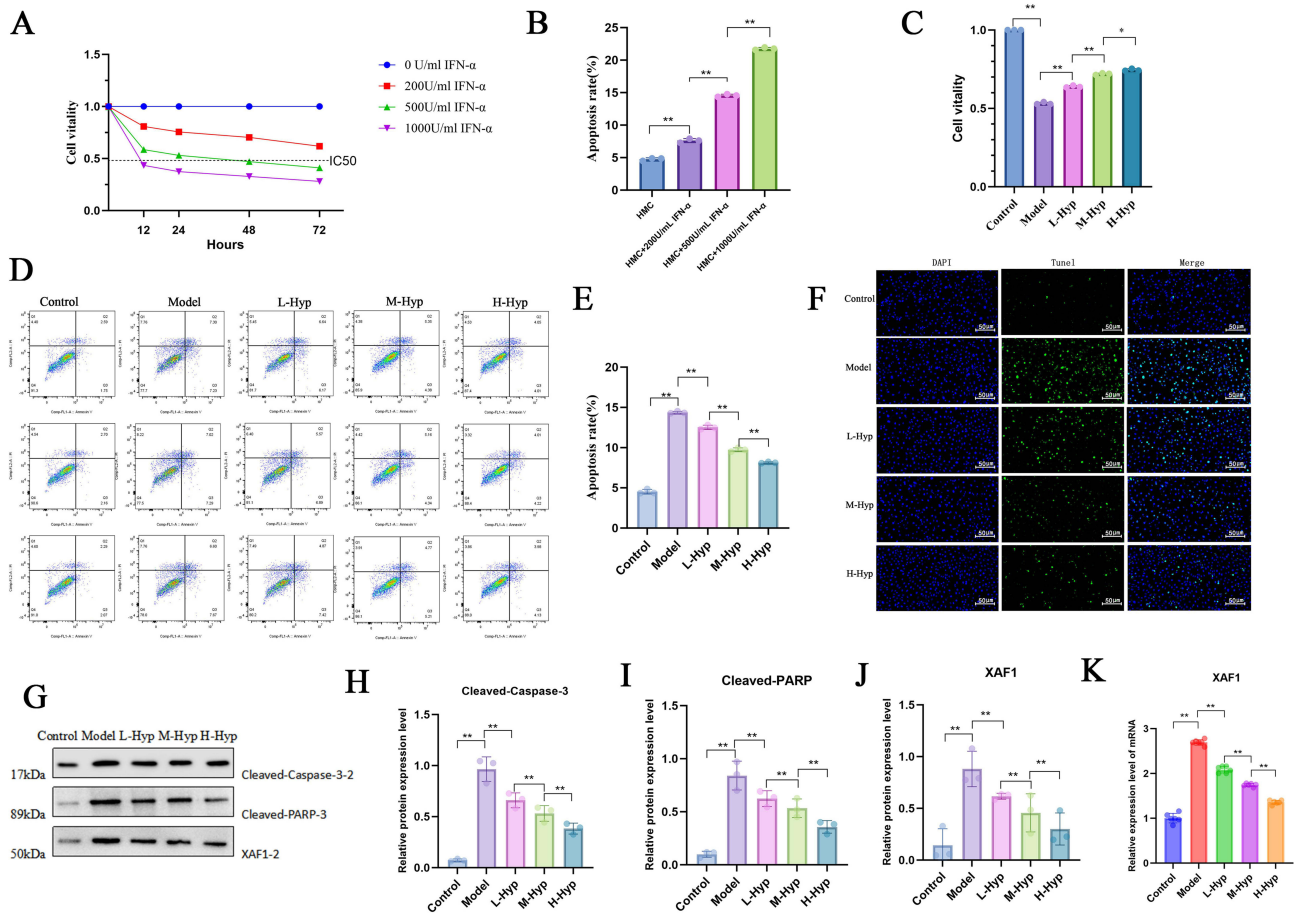

Figure 5 Hyp inhibits HMC apoptosis and XAF1 expression. (**A**) HMC cell viability under different IFN-α concentrations and times detected by CCK-8 assay; (**B**) HMC cell apoptosis rate under different IFN-α concentrations detected by flow cytometry; (**C**) Cell viability under different doses of Hyp intervention detected by CCK-8 assay; (**D**) Cell apoptosis under different doses of Hyp intervention detected by flow cytometry; (**E**) Effect of different concentrations of L-Hyp treatment on cell apoptosis rate; (**F**) Expression of cell death under different doses of Hyp intervention detected by TUNEL staining; (**G–J**) Protein expression levels of Cleaved-Caspase-3, Cleaved-PARP and XAF1 under different doses of Hyp intervention detected by Western Blot. (**K**) Effect of different doses of Hyp intervention on XAF1 expression detected by RT-PCR.*$P < 0.05$;**$P < 0.01$.

generating a large amount of XAF1 mRNA. WB results showed that knockdown of P53 reduced the protein expression of p-P53, decreased the expression of XAF1, and increased the expression of XIAP (Figure 6A–D), directly verifying that p53 is the core upstream regulatory hub of this signaling pathway.

To verify how XAF1 induces HMC cell apoptosis, we studied the role of XAF1 in regulating HMC cell apoptosis in vitro. We transfected HMC cells with XAF1-specific siRNA and pcDNA3.1 respectively, and evaluated their effects on INFa-induced cell apoptosis. Based on the transfection efficiency of si-XAF1, we selected si-XAF1 2# for subsequent experiments (Supplementary Figure 1B). CCK-8 results showed that compared with the model group, knockout of XAF1 improved cell viability, while overexpression of XAF1 significantly reduced cell viability (Figure 6E). Flow cytometry results and TUNEL staining results showed the same performance (Figure 6F and G). XAF1 can directly antagonize the apoptosis-inhibitory protein XIAP to promote apoptosis, or promote cell apoptosis by affecting the balance of Bcl-2 family proteins. WB results showed that compared with the control group, knockout of XAF1 increased the protein expression levels of Bcl-2 and XIAP, and decreased the protein expression levels of Cleaved Caspase-3 and Cleaved PARP (Figure 6H–M), indicating that P53/XAF1 is a key signaling axis mediating HMC cell apoptosis.

Hyp Attenuates XAF1-Mediated HMC Apoptosis

To further explore the mechanism by which Hyp mediates HMC apoptosis through XAF1, we set up 4 groups: Control, Model, Model+pcDNA3.1-XAF1, and Model+pcDNA3.1-XAF1+Hyp. CCK-8 study found that hyperoside can improve

 https://doi.org/10.2147/JIR.S586751

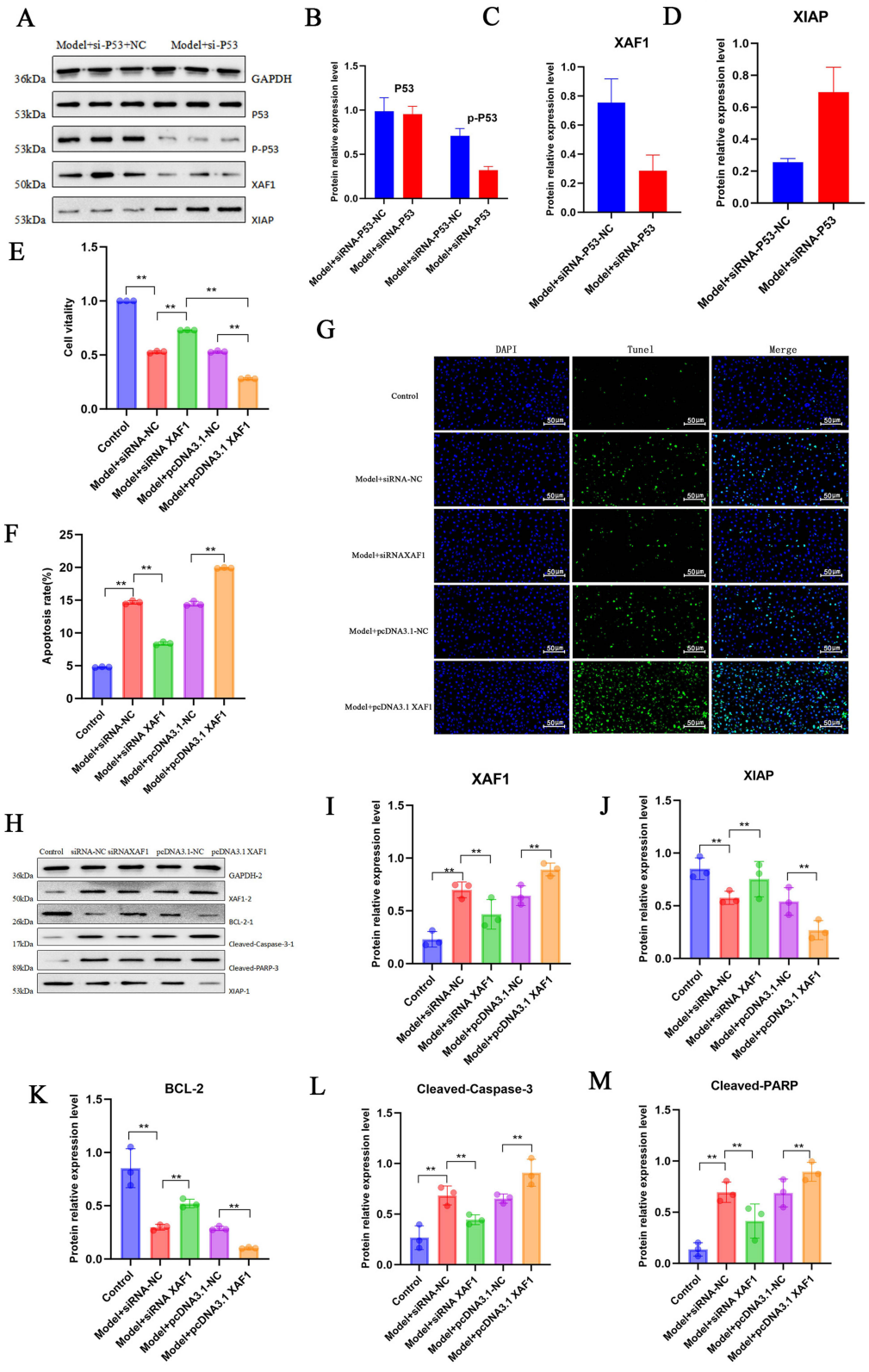

Figure 6 P53/XAF1 mediates HMC apoptosis. (**A–D**) Effects of SiRNA-P53 on the relative protein expression levels of P53, p-P53, XAF1, and XIAP detected by WB (GAPDH as internal reference); (**E**) Effect of siRNA-XAF1 or pcDNA3.1 XAF1 interference on cell viability detected by CCK-8 assay; (**F**) Effect of siRNA-XAF1 or pcDNA3.1 XAF1 interference on cell apoptosis rate detected by flow cytometry; (**G**) Effect of siRNA-XAF1 or pcDNA3.1 XAF1 interference on cell death detected by TUNEL staining; (**H–M**) Effects of siRNA-XAF1 or pcDNA3.1 XAF1 interference on the relative expression levels of XAF1, XIAP, BCL-2, Cleaved-Caspase-3, and Cleaved-PARP detected by WB.**$P < 0.01$.

https://doi.org/10.2147/JIR.S586751

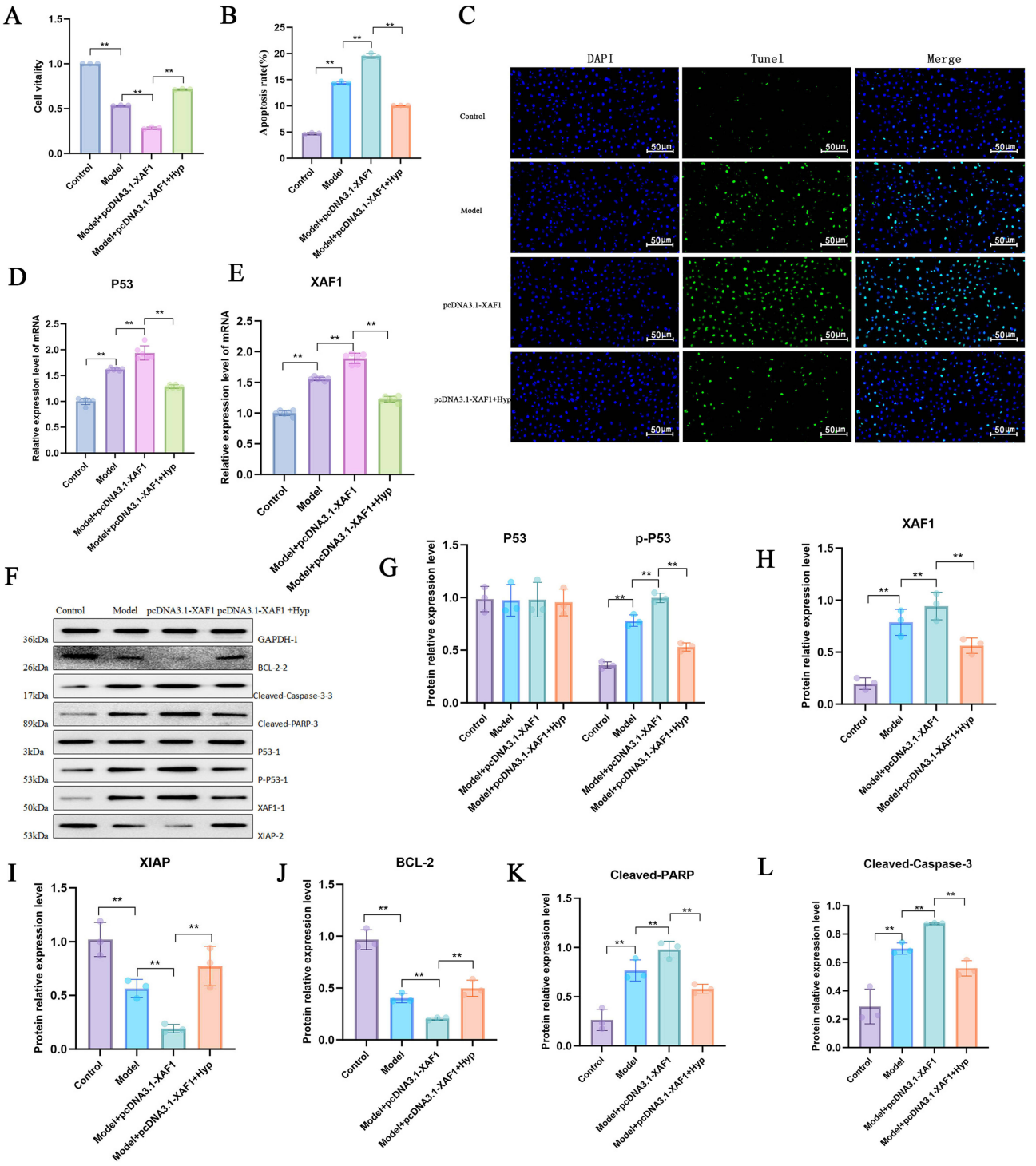

Figure 7 Hyp attenuates XAF1-mediated HMC apoptosis. (**A**) Effect of different treatment groups on cell viability detected by CCK-8 assay; (**B**) Effect of different treatment groups on cell apoptosis rate detected by flow cytometry; (**C**) Effect of different treatment groups on cell death detected by TUNEL staining; (**D**) Effect of different treatment groups on P53 mRNA expression level detected by RT-PCR; (**E**) Effect of different treatment groups on XAF1 mRNA expression level detected by RT-PCR; (**F**–**L**) Effects of different treatment groups on the protein expression levels of p-P53, XAF1, XIAP, BCL-2, Cleaved-PARP, and Cleaved-Caspase-3 detected by WB (GAPDH as internal reference).**$P < 0.01$.

the decrease in cell viability caused by XAF1 overexpression, and improve the apoptosis rate and cell death (Figure 7A–C). PCR results showed that Hyp intervention can downregulate the relative mRNA expression levels of P53 and XAF1 (Figure 7D and E). WB results showed that Hyp intervention can reduce the protein expression of p-P53, XAF1, Cleaved-

Caspase-3, and Cleaved-PARP, and increase the protein expression of XIAP and BCL-2 (Figure 7F–L). The above results indicate that Hyp inhibits the expression of apoptotic proteins Cleaved-Caspase-3 and Cleaved-PARP by inhibiting the P53/XAF1 signal and upregulating the expression of XIAP and BCL2, thereby improving the HMC apoptosis rate.

Discussion

Lupus nephritis, as one of the most severe complications of systemic lupus erythematosus, its complex immune dysregulation mechanism and abnormal apoptosis of intrinsic renal cells jointly promote disease progression, seriously threatening patients' renal function and long-term prognosis.[22] Currently, clinical reliance on corticosteroids and immunosuppressants can partially control the disease, but significant side effects limit their long-term application. Therefore, the development of new therapeutic strategies with both efficacy and safety has become an urgent clinical problem. Hyperoside, as a natural flavonoid compound, has shown multiple pharmacological activities such as anti-inflammatory, anti-apoptotic, and immunomodulatory in various autoimmune diseases and organ injury models. For example, Liu et al[10] found that Hyp can inhibit renal inflammation in diabetic nephropathy by regulating macrophage polarization; Zhang K et al[23] found that Hyp can exert a protective effect on diabetic nephropathy through the ROS-ERK signaling pathway and pyroptosis; Wei J et al[24] confirmed that Hyp induces ferroptosis in chronic myeloid leukemia cells by targeting NRF2. However, its role and molecular mechanism in LN have not been fully elucidated. This study systematically revealed the core mechanism by which Hyp inhibits glomerular mesangial cell apoptosis and improves LN by regulating the P53/XAF1 signaling pathway through multi-dimensional technologies including network pharmacology, machine learning, molecular docking, and cellular experiments, providing a new theoretical basis and experimental support for the targeted treatment of LN.

This study first identified 146 LN-related genes through integrated analysis of multiple datasets, effectively avoiding batch effects and sample bias of a single dataset, and laying a reliable disease molecular background for subsequent target screening. Potential targets of Hyp were predicted through cross-database analysis, and intersection analysis with LN-related genes obtained 18 core candidate targets of Hyp-LN, suggesting that Hyp may be involved in the pathophysiological process of LN by regulating these genes. GO and KEGG enrichment analyses showed that these candidate targets are significantly enriched in biological processes such as viral defense response, immune signal transduction, and P53 signaling pathway. Among them, the P53 signaling pathway, as a classic pathway regulating cell apoptosis,[25] its abnormal activation is closely related to the imbalance of glomerular mesangial cell apoptosis in LN. Zhao et al found that Sirt1 can protect LN by inhibiting the NLRP3 pathway, and the activation of NLRP3 inflammasome has an interactive effect with P53-mediated apoptotic signals;[7] Parodis et al also clearly proposed in a review on LN that "abnormal cell apoptosis is the core pathological link of renal injury in LN, and abnormal P53 pathway is one of the key driving factors", which is highly consistent with the enrichment results of this study,[4] initially suggesting that the P53-mediated apoptotic pathway may be the key pathway for Hyp to exert its effects.

To further screen the core targets of Hyp in the treatment of LN, this study constructed an integrated machine learning model including 9 algorithms such as RF, XGBoost, and SVM, combined with SHAP interpretability analysis, and successfully identified 5 core genes including STAT1, RSAD2, OAS3, GBP1, and XAF1. This screening strategy is significantly superior to traditional single-algorithm models, consistent with the concept of "improving the accuracy of core target screening through multi-algorithm integration" mentioned by Shao et al[21] From the perspective of domestic and foreign research progress, STAT1, as a key molecule in the type I interferon signaling pathway,[26] its high expression has been repeatedly confirmed in the renal tissue of LN patients;[27,28] RSAD2 and OAS3 are interferon-induced antiviral proteins. Studies have found that targeting the pathogenic interferon-stimulated gene RSAD2 improves pregnancy outcomes in systemic lupus erythematosus models,[29] and OAS3 negatively regulates the expression of chemokines and interferon-responsive genes in human macrophages.[30] As a key downstream molecule of the P53 signaling pathway, XAF1 not only shows a clear functional contribution in SHAP analysis,[31] but also molecular docking verification shows that Hyp has an extremely strong binding affinity with XAF1 (binding energy up to −44.6 kcal/mol), which is significantly higher than other core genes, suggesting that XAF1 may be the core target directly acted by Hyp.

From the research progress of XAF1, its role as an apoptosis-regulating protein has been extensively explored in various diseases. XAF1 can antagonize the inhibitory effect of XIAP on Caspase family proteins by binding to the BIR

domain of the apoptosis-inhibitory protein XIAP, thereby relieving the apoptosis-inhibitory signal;[32–34] at the same time, XAF1 can also promote the mitochondrial localization of the pro-apoptotic protein Bax by regulating the balance of Bcl-2 family proteins, aggravate mitochondrial damage and cytochrome C release, and ultimately initiate the apoptotic cascade reaction.[35,36] In the field of renal diseases, Qiu et al found that silencing the XAF1 gene in renal tissue reduced glomerular mesangial cell apoptosis, secondary glomerular mesangial cell proliferation, and urinary protein secretion in Thy-1N rats in the study of human mesangial proliferative glomerulonephritis.[37] However, the role of XAF1 in LN-related research has not been clarified before. This study first associates XAF1 with glomerular mesangial cell apoptosis in LN, filling this research gap. In addition, the mechanism by which XAF1 expression is regulated by P53 transcription has been confirmed in tumor research. As a tumor suppressor gene, P53 can directly drive the transcriptional expression of XAF1 by binding to the P53 response element (RE) in the promoter region of the XAF1 gene,[38] which provides a key theoretical basis for the subsequent exploration of the role of the P53/XAF1 signaling axis in this study.

In vitro cellular experiments further verified the above mechanism hypothesis. This study used IFN-α induction to establish an HMC cell apoptosis model,[39] simulating the damaging effect of inflammatory mediators on glomerular mesangial cells under LN pathological conditions. This model selection has clear clinical relevance,[40] because the serum IFN-α level in LN patients is significantly increased, and IFN-α can induce glomerular mesangial cell apoptosis by activating the JAK-STAT pathway.[41] Experimental results showed that Hyp intervention can increase HMC cell viability and reduce apoptosis rate in a dose-dependent manner, while significantly downregulating the expression of apoptosis-related proteins Cleaved-Caspase-3 and Cleaved-PARP, confirming the inhibitory effect of Hyp on LN-related glomerular mesangial cell apoptosis. More importantly, the mRNA and protein expressions of XAF1 were significantly reduced after Hyp intervention in a dose-dependent manner, directly linking the regulatory relationship between Hyp and the core target XAF1.

To clarify the function of the P53/XAF1 signaling axis, this study knocked down P53 expression by siRNA and found that XAF1 expression decreased accordingly, while XIAP expression increased, confirming the transcriptional regulatory effect of P53 on XAF1 in the LN model, which is consistent with the previous expression results. Further verification of the key role of XAF1 in HMC cell apoptosis through XAF1 knockdown and overexpression experiments: XAF1 knockdown can significantly improve IFN-α induced cell apoptosis, while XAF1 overexpression exacerbates cell apoptosis, accompanied by downregulation of Bcl-2 and XIAP expression and upregulation of Cleaved-Caspase-3 and Cleaved-PARP expression, clarifying that XAF1 is a key molecule mediating HMC cell apoptosis. Finally, rescue experiments confirmed that Hyp can effectively reverse the exacerbated HMC cell apoptosis caused by XAF1 overexpression, while downregulating the phosphorylation level of P53 and the expression of XAF1, and upregulating the expression of XIAP and Bcl-2, verifying from both positive and negative aspects that Hyp exerts a protective effect on glomerular mesangial cells by inhibiting the P53/XAF1 signaling pathway and regulating the expression of downstream apoptosis-related proteins.

The innovations of this study are mainly reflected in three aspects: First, the systematic research strategy of "multi-dataset integration - network pharmacology - machine learning - SHAP analysis - molecular docking - cellular experiments" is adopted to realize the full-chain exploration from target prediction, core screening to mechanism verification, which significantly improves the reliability and persuasiveness of the research conclusions, and is highly consistent with the development trend of "multi-disciplinary integration" in current biomedical research; second, it is the first to clarify that XAF1 is the core target of Hyp in the treatment of LN, and confirms that the P53/XAF1 signaling axis is the key pathway for Hyp to inhibit glomerular mesangial cell apoptosis, filling the research gap in the mechanism of Hyp in LN, and providing a new molecular explanation for the pathogenesis of LN; third, breaking the "black box" limitation of traditional machine learning models through SHAP analysis, quantifying the contribution and regulatory direction of core genes to disease prediction, and providing a new technical idea for the screening of LN diagnostic markers.

From a translational perspective, B-cell–targeted therapies have been increasingly evaluated in LN, including anti-CD20 monoclonal antibodies in adults (eg, obinutuzumab added to MMF plus glucocorticoids in a Phase 3 trial)[42] and rituximab-based regimens, where the degree and durability of peripheral B-cell depletion has been associated with renal response.[43] In paediatric/childhood-onset LN, rituximab combined with MMF has also been

reported in clinical cohorts.[44] Although our study did not directly evaluate treatment response, these clinical observations are conceptually consistent with our mechanistic finding that IFN-α–driven apoptotic stress activates the P53/XAF1 axis in mesangial cells, which can be mitigated by Hyp; B-cell–directed therapies may reduce upstream autoantibody/immune-complex formation and type I IFN signalling, thereby indirectly dampening XAF1-associated apoptosis. Future multi-omic studies linking B-cell–modulating therapies with tissue- and cell-type–resolved expression of XAF1 and related apoptotic signatures in both adults and children are warranted.

At the same time, this study also has limitations: First, the public transcriptomic cohorts integrated in this study predominantly represent adult-onset SLE/LN and do not include dedicated paediatric/childhood-onset lupus nephritis cohorts; given the distinct clinical behaviour and potentially different molecular drivers in paediatric LN, extrapolation to children should be made with caution, and future work should validate and compare age-stratified signatures in paediatric cohorts.[13] Second, treatment regimens, therapeutic response (eg, remission status) and longitudinal renal outcomes were not consistently available across the public gene-expression datasets analysed; therefore, we could not correlate the investigated genes (including XAF1) with treatment response or prognosis in this study. Future studies integrating transcriptomic profiles with standardized clinical metadata and follow-up outcomes will be important to assess the predictive value of these genes for therapeutic response and renal survival. Third, in vitro cellular experiments only simulate part of the LN pathological state, lacking in vivo animal model verification - subsequent studies need to further confirm the regulatory effect of Hyp on renal function (such as serum creatinine, urinary protein), pathological damage (glomerular mesangial proliferation, immune complex deposition) and the P53/XAF1 signaling pathway through MRL/lpr lupus mice or pristane-induced LN rat models, which is a key step to promote the clinical transformation of Hyp; Fourth, this study focuses on glomerular mesangial cells, while LN pathological damage involves various cell types such as immune cells (such as macrophages, T cells) and renal tubular epithelial cells. Whether Hyp has a regulatory effect on other cell types and whether other potential signaling pathways (such as NF-κB, MAPK pathways) are involved in its therapeutic effect still need further exploration; Fifth, Our data suggest that hyperoside may exert a kidney-intrinsic cytoprotective effect by reducing mesangial-cell apoptosis via the p53/XAF1 axis. Several of the identified core genes (eg, XAF1/STAT1/RSAD2/OAS3/GBP1) are interferon-stimulated genes, providing a plausible intersection between immune-modulating therapies and the IFN-α–driven injury context modeled here[45,46] however, direct clinical-response associations require dedicated cohort studies. Mechanistically, p53 is known to transcriptionally regulate pro-apoptotic programs,[32] and our results are consistent with p53 acting upstream of XAF1. Hyperoside may decrease XAF1 expression largely by suppressing p53 activation under IFN-α stimulation. We also acknowledge that XAF1 could be regulated by p53-independent pathways in inflammatory settings.[47,48] Future work such as ChIP-qPCR assessing p53 binding at the XAF1 promoter and pharmacologic/overexpression rescue experiments will help distinguish direct versus indirect regulation.

Conclusion

This study integrated public transcriptomic analyses with in vitro experiments to identify XAF1 as a potential hyperoside-associated target relevant to lupus nephritis and to demonstrate that hyperoside reduces IFN-α–induced mesangial-cell apoptosis via suppression of the p53/XAF1 axis. In the future, in vivo studies and clinical datasets are needed to confirm efficacy and translational relevance.

Data Sharing Statement

All datasets generated and analyzed during this study are included in this published article and its supplementary materials.

Author Contributions

LLC: Writing – original draft, Methodology, Analysis. ZFT: Visualization; Software; Data Curation. JJC: execution. ML: Writing – review & editing; Data Curation. CBH: Project administration, Conceptualization. All authors took part in drafting, revising, or critically reviewing the article; gave final approval of the version to be published; have agreed on the journal to which the article has been submitted; and agree to be accountable for all aspects of the work.

Funding

This work was supported by the National Natural Science Foundation of China General Program (82574970); Major and Difficult Diseases Clinical Research Project on Collaboration between Traditional Chinese and Western Medicine (ZDYN-2024-A-146); Anhui Provincial Clinical Medicine Research and Transformation Special Projects (202304295107020114, 202304295107020115); Institute of Xin'an Medicine and Modernization of Traditional Chinese Medicine, Great Health Research Institute Special Projects (2023CXMMTCM015, 2023CXMMTCM004); Anhui Provincial Graduate Quality Engineering Graduate Innovation and Entrepreneurship Practice Project (2024cxcysj121); 2024 Anhui Provincial Higher Education Institutions Key Scientific Research Project (2024AH050957); 2024 Anhui Provincial Health Commission Scientific Research Project (2024Aa30428). The funding agencies had no role in the study design, data collection and analysis, decision to publish, or preparation of the manuscript.

Disclosure

The authors declare that the research was conducted in the absence of any commercial or financial relationships that could be construed as a potential conflict of interest.

References

1. Yu C, Li P, Dang X, Zhang X, Mao Y, Chen X. Lupus nephritis: new progress in diagnosis and treatment. *J Autoimmun*. 2022;132:102871. doi:10.1016/j.jaut.2022.102871
2. Roveta A, Parodi EL, Brezzi B, et al. Lupus nephritis from pathogenesis to new therapies: an update. *Int J Mol Sci*. 2024;25(16). doi:10.3390/ijms25168981
3. Gasparotto M, Gatto M, Binda V, Doria A, Moroni G. Lupus nephritis: clinical presentations and outcomes in the 21st century. *Rheumatology*. 2020;59(Suppl5):v39–v51. doi:10.1093/rheumatology/keaa381
4. Parodis I, Rovin BH, Tektonidou MG, et al. Lupus nephritis. *Nat Rev Dis Primers*. 2025;11(1):69. doi:10.1038/s41572-025-00653-y
5. Siegel CH, Sammaritano LR. Systemic lupus erythematosus: a review. *JAMA*. 2024;331(17):1480–1491. doi:10.1001/jama.2024.2315
6. Li W, Yao C, Guo H, et al. Macrophages communicate with mesangial cells through the CXCL12/DPP4 axis in lupus nephritis pathogenesis. *Cell Death Dis*. 2024;15(5):344. doi:10.1038/s41419-024-06708-4
7. Zhao Y, Zhang AP, Bao BY, Fan H, Yang XY. Sirt1 protects lupus nephritis by inhibiting the NLRP3 signaling pathway in human glomerular mesangial cells. *Open Life Sci*. 2025;20(1):20221038. doi:10.1515/biol-2022-1038
8. Maurya SK, Divakar S, Rathee S, Patil UK. Diverse therapeutic potentials of hypericin: an in-depth review. *Curr Top Med Chem*. 2025;25(21):2478–2512. doi:10.2174/0115680266330142250224101958
9. Wang Q, Wei HC, Zhou SJ, et al. Hyperoside: a review on its sources, biological activities, and molecular mechanisms. *Phytother Res*. 2022;36(7):2779–2802. doi:10.1002/ptr.7478
10. Liu J, Zhang Y, Sheng H, et al. Hyperoside suppresses renal inflammation by regulating macrophage polarization in mice with type 2 diabetes mellitus. *Front Immunol*. 2021;12:733808. doi:10.3389/fimmu.2021.733808
11. Chen L, Qin Z, Ruan ZB. Hyperoside alleviates doxorubicin-induced myocardial cells apoptosis by inhibiting the apoptosis signal-regulating kinase 1/p38 pathway. *PeerJ*. 2023;11:e15315. doi:10.7717/peerj.15315
12. Clough E, Barrett T, Wilhite SE, et al. NCBI GEO: archive for gene expression and epigenomics data sets: 23-year update. *Nucleic Acids Res*. 2024;52(D1):D138–D144. doi:10.1093/nar/gkad965
13. Chan EY, Marks SD. Childhood-onset lupus nephritis: unique aspects and challenges in management. *Kidney Int*. 2025;108(5):799–810. doi:10.1016/j.kint.2025.05.039
14. Hähnke VD, Kim S, Bolton EE. PubChem chemical structure standardization. *J Cheminform*. 2018;10(1):36. doi:10.1186/s13321-018-0293-8
15. Hunter FMI, Ioannidis H, Bento AP, et al. Drug and clinical candidate drug data in ChEMBL. *J Med Chem*. 2025;68(19):19800–19827. doi:10.1021/acs.jmedchem.5c00920
16. Daina A, Michielin O, Zoete V. SwissTargetPrediction: updated data and new features for efficient prediction of protein targets of small molecules. *Nucleic Acids Res*. 2019;47(W1):W357–W364. doi:10.1093/nar/gkz382
17. Wang Z, Liang L, Yin Z, Lin J. Improving chemical similarity ensemble approach in target prediction. *J Cheminform*. 2016;8(1):20. doi:10.1186/s13321-016-0130-x
18. Liu S, Wang Z, Zhu R, Wang F, Cheng Y, Liu Y. Three differential expression analysis methods for RNA sequencing: limma, EdgeR, DESeq2. *J Vis Exp*. 2021;175. doi:10.3791/62528
19. Langfelder P, Horvath S. WGCNA: an R package for weighted correlation network analysis. *BMC Bioinf*. 2008;9(1):559. doi:10.1186/1471-2105-9-559
20. Wu T, Hu E, Xu S, et al. clusterProfiler 4.0: a universal enrichment tool for interpreting omics data. *Innovation*. 2021;2(3):100141. doi:10.1016/j.xinn.2021.100141
21. Shao Z, Deng Q, Cheng L, et al. Lactylation-related gene AKR1A1 contributes to osteoporosis via metabolic-immune regulation: evidence from multi-omics integration, single-cell transcriptomics, and in vitro validation. *Front Immunol*. 2025;16:1680305. doi:10.3389/fimmu.2025.1680305
22. Mistry P, Kaplan MJ. Cell death in the pathogenesis of systemic lupus erythematosus and lupus nephritis. *Clin Immunol*. 2017;185:59–73. doi:10.1016/j.clim.2016.08.010

23. Zhang K, Li M, Yin K, et al. Hyperoside mediates protection from diabetes kidney disease by regulating ROS-ERK signaling pathway and pyroptosis. *Phytother Res*. 2023;37(12):5871–5882. doi:10.1002/ptr.7993
24. Wei J, Chai Q, Qin Y, et al. Hyperoside induces ferroptosis in chronic myeloid leukemia cells by targeting NRF2. *Mol Med*. 2024;30(1):224. doi:10.1186/s10020-024-01002-7
25. Wang H, Guo M, Wei H, Chen Y. Targeting p53 pathways: mechanisms, structures, and advances in therapy. *Signal Transduct Target Ther*. 2023;8(1):92. doi:10.1038/s41392-023-01347-1
26. Gallucci S, Meka S, Gamero AM. Abnormalities of the type I interferon signaling pathway in lupus autoimmunity. *Cytokine*. 2021;146:155633. doi:10.1016/j.cyto.2021.155633
27. Cai Z, Zhang S, Wu P, et al. A novel potential target of IL-35-regulated JAK/STAT signaling pathway in lupus nephritis. *Clin Transl Med*. 2021;11(2):e309. doi:10.1002/ctm2.309
28. Zheng C, Shang F, Cheng R, Bai Y. STAT1 aggravates kidney injury by NOD-like receptor (NLRP3) signaling in MRL-lpr mice. *J Mol Histol*. 2024;55(4):555–566. doi:10.1007/s10735-024-10208-2
29. Negatu SG, Jurado KA. Targeting pathogenic interferon-stimulated gene RSAD2 improves pregnancy outcomes in systemic lupus erythematosus models. *Cell Rep Med*. 2025;6(3):102034. doi:10.1016/j.xcrm.2025.102034
30. Lee WB, Choi WY, Lee DH, Shim H, Kim-Ha J, Kim YJ. OAS1 and OAS3 negatively regulate the expression of chemokines and interferon-responsive genes in human macrophages. *BMB Rep*. 2019;52(2):133–138. doi:10.5483/BMBRep.2019.52.2.129
31. Pinto EM, Figueiredo BC, Chen W, et al. XAF1 as a modifier of p53 function and cancer susceptibility. *Sci Adv*. 2020;6(26):eaba3231. doi:10.1126/sciadv.aba3231
32. Zou B, Chim CS, Pang R, et al. XIAP-associated factor 1 (XAF1), a novel target of p53, enhances p53-mediated apoptosis via post-translational modification. *Mol Carcinog*. 2012;51(5):422–432. doi:10.1002/mc.20807
33. Liston P, Fong WG, Kelly NL, et al. Identification of XAF1 as an antagonist of XIAP anti-Caspase activity. *Nat Cell Biol*. 2001;3(2):128–133. doi:10.1038/35055027
34. Zhang M, Huang Y, Bai J, et al. XAF1 promotes osteoclast apoptosis by antagonizing the XIAP-caspase axis. *J Orthop Translat*. 2024;47:15–28. doi:10.1016/j.jot.2024.05.001
35. Park GB, Park SH, Kim D, Kim YS, Yoon SH, Hur DY. Berberine induces mitochondrial apoptosis of EBV-transformed B cells through p53-mediated regulation of XAF1 and GADD45α. *Int J Oncol*. 2016;49(1):411–421. doi:10.3892/ijo.2016.3502
36. Straszewski-Chavez SL, Visintin IP, Karassina N, et al. XAF1 mediates tumor necrosis factor-alpha-induced apoptosis and X-linked inhibitor of apoptosis cleavage by acting through the mitochondrial pathway. *J Biol Chem*. 2007;282(17):13059–13072. doi:10.1074/jbc.M609038200
37. Qiu W, Zhou J, Zhu G, et al. Sublytic C5b-9 triggers glomerular mesangial cell apoptosis via XAF1 gene activation mediated by p300-dependent IRF-1 acetylation. *Cell Death Dis*. 2014;5(4):e1176. doi:10.1038/cddis.2014.153
38. Zhang W, Guo Z, Jiang B, et al. Identification of a functional p53 responsive element within the promoter of XAF1 gene in gastrointestinal cancer cells. *Int J Oncol*. 2010;36(4):1031–1037. doi:10.3892/ijo_00000584
39. Li M, Yu D, Wang Y, Luo N, Han G, Yang B. Interferon-α activates interleukin-1 receptor-associated kinase 1 to induce regulatory T-cell apoptosis in patients with systemic lupus erythematosus. *J Dermatol*. 2021;48(8):1172–1185. doi:10.1111/1346-8138.15899
40. Whittall Garcia LP, Gladman DD, Urowitz M, et al. Interferon-α as a biomarker to predict renal outcomes in lupus nephritis. *Lupus Sci Med*. 2024;11(2). doi:10.1136/lupus-2024-001347
41. Dong J, Wang QX, Zhou CY, Ma XF, Zhang YC. Activation of the STAT1 signalling pathway in lupus nephritis in MRL/lpr mice. *Lupus*. 2007;16(2):101–109. doi:10.1177/0961203306075383
42. Furie RA, Rovin BH, Garg JP, et al. Efficacy and safety of obinutuzumab in active lupus nephritis. *N Engl J Med*. 2025;392(15):1471–1483. doi:10.1056/NEJMoa2410965
43. Gomez Mendez LM, Cascino MD, Garg J, et al. Peripheral blood B cell depletion after rituximab and complete response in lupus nephritis. *Clin J Am Soc Nephrol*. 2018;13(10):1502–1509. doi:10.2215/cjn.01070118
44. Hogan J, Godron A, Baudouin V, et al. Combination therapy of rituximab and mycophenolate mofetil in childhood lupus nephritis. *Pediatr Nephrol*. 2018;33(1):111–116. doi:10.1007/s00467-017-3767-4
45. Leaman DW, Chawla-Sarkar M, Vyas K, et al. Identification of X-linked inhibitor of apoptosis-associated factor-1 as an interferon-stimulated gene that augments TRAIL Apo2L-induced apoptosis. *J Biol Chem*. 2002;277(32):28504–28511. doi:10.1074/jbc.M204851200
46. Juraleviciute M, Nsengimana J, Newton-Bishop J, Hendriks GJ, Slipicevic A. MX2 mediates establishment of interferon response profile, regulates XAF1, and can sensitize melanoma cells to targeted therapy. *Cancer Med*. 2021;10(8):2840–2854. doi:10.1002/cam4.3846
47. Jeong SI, Kim JW, Ko KP, et al. XAF1 forms a positive feedback loop with IRF-1 to drive apoptotic stress response and suppress tumorigenesis. *Cell Death Dis*. 2018;9(8):806. doi:10.1038/s41419-018-0867-4
48. Nishimura Y, Iwashita M, Hayashi M, et al. XAF1 overexpression exacerbates diabetes by promoting pancreatic β-cell apoptosis. *Acta Diabetol*. 2022;59(10):1275–1286. doi:10.1007/s00592-022-01930-y